Biophysical Chemistry 152 (2010) 99–108

Contents lists available at ScienceDirect

Biophysical Chemistry

journal homepage: http://www.elsevier.com/locate/biophyschem

Conformational selection, dynamic restriction and the hydrophobic effect coupled to stabilization of the BIR3 domain of the human X-linked inhibitor of apoptosis protein by the tetrapeptide AVPI

Theo Luiz Ferraz de Souza [a], Daniel Sanches [a], Rafael Braga Gonçalves [a], Samuel Silva da RochaPita [b], Pedro Geraldo Pascutti [b], M. Lucia Bianconi [a], Fabio Ceneviva Lacerda de Almeida [a], Jerson L. Silva [a], Andréa Cheble de Oliveira [a,*]

[a] Programa de Biologia Estrutural and Centro Nacional de Ressonância Magnética Nuclear de Macromoléculas, Instituto de Bioquímica Médica, Instituto Nacional de Ciência e Tecnologia de Biologia Estrutural e Bioimagem, INBEB, Universidade Federal do Rio de Janeiro, Rio de Janeiro, RJ, 21941-902, Brazil
[b] Laboratório de Modelagem e Dinâmica Molecular (LMDM), Instituto de Biofísica Carlos Chagas Filho, Universidade Federal do Rio de Janeiro, Rio de Janeiro, RJ, 21941-590, Brazil

ARTICLE INFO

Article history:
Received 1 July 2010
Received in revised form 9 August 2010
Accepted 10 August 2010
Available online 17 August 2010

Keywords:
XIAP-BIR3/AVPI interaction
Protein stability
Thermodynamics
Spectroscopy
Calorimetry
Apoptosis

ABSTRACT

The XIAP-BIR3 domain blocks a substantial portion of the apoptosis pathway and is an attractive target for novel anticancer agents. The tetrapeptide AVPI, from the protein Smac/DIABLO, binds to the XIAP-BIR3 domain, allowing the cancer cells to die. Here we characterize the binding parameters of AVPI to XIAP-BIR3 and analyze its effects on the thermodynamic stability of this domain. XIAP-BIR3 was exceptionally stable against physical and chemical treatments and became even more stable by interaction with AVPI. Nuclear magnetic resonance experiments demonstrated that conformational selection is taking place upon AVPI interaction with XIAP-BIR3. Molecular dynamics simulations corroborate that the flexibility of XIAP-BIR3 is significantly reduced. The positive binding entropy associated with a loss of conformational entropy involved in the binding indicates that hydrophobic interactions play an important role in the interaction and domain stabilization. The mechanism of XIAP-BIR3 stabilization and its implications for drug affinity optimization are discussed.

1. Introduction

Apoptosis is a process essential for the development and homeostasis of multicellular organisms, and it can lead to a variety of diseases, such as neurodegenerative disorders and cancer, when deregulated [1–3]. Inhibitors of apoptosis proteins (IAPs) are members of an important class of endogenous proteins that can inhibit apoptosis in both intrinsic and extrinsic pathways [4,5]. Among the IAPs that have been studied, the human X-linked IAP (XIAP) appears to be the most potent, and it plays a key role in binding to and inhibiting an initiator caspase (caspase-9) and two effector caspases (caspase-3 and caspase-7) [6–9].

All members of the IAP family present at least one baculoviral IAP repeat (BIR) motif, although many of them contain three motifs. XIAP is a single protein that has three BIR domains and a C-terminal RING finger that are specific for different caspases [10]. Analyses of the structure and function of XIAP have demonstrated that the third BIR domain (BIR3) inhibits caspase-9 selectively and that the inhibition of caspase-3 and 7 is mediated by the linker region between BIR1 and BIR2 [6,7,9,11,12]. The interaction between XIAP and the caspases can be inhibited by Smac/DIABLO, a second mitochondrial activator of the caspases/direct IAP-binding protein, which is released from mitochondria upon initiation of the apoptotic signaling process [13–16]. Structural and biological studies have shown that the interaction between XIAP and Smac/DIABLO takes place between a well-defined surface groove in the BIR3 domain of XIAP and four amino acid residues (AVPI, i.e., Ala-Val-Pro-Ile) at the N-terminus of Smac/DIABLO [14,15]. This four-residue binding motif (i.e., the IAP-binding motif, IBM), is present both in human and mouse caspase-9 [17].

Excessive expression of XIAP and other IAPs occurs in several types of human cancer cells [18–20] and predicts a worse prognosis [21]. Several studies have demonstrated that XIAP plays a critical role in the resistance of cancer cells to chemotherapeutic agents, radiation, and other treatments [22–24]. Thus, different approaches to the inhibition of the antiapoptotic function of XIAP have been explored recently, including the use of antisense oligonucleotides [25] and XIAP inhibitors [26,27]. The tetrapeptide AVPI (from Smac/DIABLO) and other synthetic Smac peptides are able to interact with the XIAP-BIR3 domain, thereby

Abbreviations: BIR, baculoviral IAP repeat; caspase, cysteinyl aspartate-specific proteinase; CD, circular dichroism; Cyt c, cytochrome c; DIABLO, **D**irect **IA**P **B**inding protein with **LO**w pI; IPTG, isopropylthiogalactoside; LB, Luria–Bertani; Smac, **S**econd **M**itochondria-derived **A**ctivator of **C**aspases; UV, ultraviolet.

* Corresponding author. Mailing Address: Av. Carlos Chagas Filho 373, CCS/IBqM/ Bloco E, sala 08, Cidade Universitária, CEP 21941-902, Rio de Janeiro, RJ, Brazil. Tel.: +5521 2562 6756.
E-mail address: cheble@bioqmed.ufrj.br (A.C. de Oliveira).

0301-4622/$ – see front matter © 2010 Elsevier B.V. All rights reserved.
doi:10.1016/j.bpc.2010.08.005

inhibiting XIAP and increasing the sensitivity of cancer cells to chemotherapeutic agents both *in vitro* [28,29] and *in vivo* [28–30]. Therefore, several of these approaches have been undertaken to understand the interaction between XIAP-BIR3 and AVPI. Different techniques, including nuclear magnetic resonance [14], crystallography [15] and fluorescence polarization [15,26], have already provided essential data regarding this interaction. Novel anti-IAP candidate drugs have been designed based on the interaction between XIAP-BIR3 and AVPI [31]. However, the thermodynamic aspects of this interaction have not been studied in depth. Many biological processes depend strictly on the thermodynamic stability of the interacting biomolecules [32–37]. In addition, detailed information of the structural-thermodynamic relationships of protein–ligand interactions is of great benefit to structure-based drug design [35]. A better understanding of the structural, dynamic and thermodynamic contributions involved in the formation of the XIAP-BIR3/AVPI complex can provide some insights for drug affinity optimization.

Here, we investigate the binding of AVPI to the XIAP-BIR3 domain to analyze its effects on the thermodynamic stability of this domain using fluorescence spectroscopy, circular dichroism, and calorimetry. We find that the XIAP-BIR3 domain is highly stabilized against urea and thermal denaturation upon interaction with the tetrapeptide AVPI. Nuclear magnetic resonance and molecular dynamics simulations were also used to assist us in understanding the effects of AVPI on the structure and dynamics of the XIAP-BIR3 domain. We determined the thermodynamic parameters of the association between XIAP-BIR3 and AVPI, such as the enthalpy (ΔH), entropy (ΔS), Gibbs free energy (ΔG) and heat capacity (ΔC_p) changes using isothermal titration calorimetry (ITC). We also calculated the unfolding parameters (ΔG, [$U_{1/2}$], and T_m) of XIAP-BIR3 and verified the changes after binding to AVPI. The molecular mechanisms of XIAP-BIR3 stabilization and the implications for drug design are discussed.

2. Materials and methods

2.1. Chemicals

All reagents were of analytical grade. Experiments were performed in the standard buffer: 15 mM Tris, pH 7.4, containing 150 mM NaCl and 1 mM DTT.

2.2. Protein preparation

The recombinant XIAP-BIR3 domain (residues 238–358) was overexpressed in *Escherichia coli* strain BL21 (DE3) as C-terminal GST-fusion proteins using the pGEX-2 T vector (Pharmacia) in LB medium at 37 °C. This plasmid containing the XIAP-BIR3 sequence was kindly provided by Dr. Yigong Shi [15]. Expression of the protein was induced with 2 mM IPTG. Five hours after induction, the cells were centrifuged (6000 r.p.m. for 20 min; RPR 9.2 rotor; Beckman) at 4 °C and frozen overnight at −20 °C. After thawing, the cells were resuspended in lysis buffer (100 mM Na_2HPO_4, 2.7 mM Na_2HPO_4, 100 mM NaCl, 2.7 mM KCl and 1 mM DTT, pH 7.4) and sonicated. The cell debris was pelleted by centrifugation (15,000 r.p.m. for 20 min; RPR 20.2 rotor; Beckman). The supernatant was applied to a GST affinity column and washed with binding buffer, and the protein was eluted with 10 mM reduced glutathione. After purification, the GST tag was removed using thrombin, and this was followed by a second round of purification using the same column. The purity of the product was confirmed using high-performance liquid chromatography (Superdex-75 column from Pharmacia, data not shown). The samples were dialyzed against the standard buffer (15 mM Tris–HCl, 150 mM NaCl and 1 mM DTT, pH 7.4).

2.3. High pressure and fluorescence spectroscopy

The high-pressure vessel that we used has been described by Paladini and Weber and was purchased from ISS Inc. (Champaign, IL). Fluorescence emission measurements were recorded using an ISSK2 spectrofluorometer (ISS Inc., Champaign, IL). The intrinsic fluorescence was excited at 280 nm, and the emission was observed from 300 to 420 nm. Changes in the fluorescence spectra at pressure p were evaluated based on changes in the spectral center of mass, $\langle \upsilon_p \rangle$:

$$\langle \upsilon_p \rangle = \Sigma \upsilon_i F_i / \Sigma F_i \quad (1)$$

F_i represents the fluorescence emitted at wavenumber υ_i, and the summation was carried out over the range of appreciable values of F.

2.4. Chemical denaturation

The samples were incubated with increasing concentrations of urea (0.5 to 9.3 M) and allowed to equilibrate overnight at 25 °C before measuring the ellipticity in the presence and absence of the denaturant. Each experiment was performed at least three times with different protein preparations.

The free energy change can be correlated empirically using the following equation [38]:

$$\Delta G^0_{[u]} = \Delta G^0_{[0M]} - m[\text{Urea}] \quad (2)$$

$\Delta G^0_{[u]}$ is the apparent free energy of unfolding at each [Urea], $\Delta G^0_{[0M]}$ is the free energy of unfolding in the absence of denaturant, and m is the proportionality constant. The parameter $\Delta G^0_{[u]}$ can be described in the equation $\Delta G^0_{[u]} = -RT \ln K_u$, where R is the gas constant, and T is the absolute temperature in Kelvin. The unfolding constant (K_u) at each urea concentration was determined using the equation $K_u = [(\alpha_u)/(1-\alpha_u)]$, where the values of α_u correspond the fraction of unfolded protein [39].

2.5. Circular dichroism spectroscopy (CD)

CD spectra were recorded using a Jasco J-715 1505 spectropolarimeter. The XIAP-BIR3 samples were diluted to a final concentration of the standard buffer. The spectra were obtained using a 0.01-cm path length quartz cuvette. The spectra were averaged from three scans that were recorded at 50 nm/min and are representative of three independent experiments. The CD spectra of the buffer or AVPI in buffer were subtracted from the respective raw data. Only the far UV region (190 to 260 nm) was analyzed.

2.6. Isothermal titration calorimetry (ITC)

ITC measurements were performed using a VP-ITC calorimeter from MicroCal, Llc. (Northampton, MA). The titration of 10 μM BIR3 with AVPI involved 18 injections (10 × 3 μL and 8 × 7.5 μL) of 0.933 M AVPI solution at 5-min intervals with constant stirring at 400 rpm. The temperature was set at 10, 25 or 37 °C. The BIR3 solutions were degassed under vacuum before the titrations, and the reference cell was filled with Milli-Q water. The heat of dilution of AVPI into the buffer was subtracted from the raw data obtained using XIAP-BIR3. The data were analyzed using the Origin 7.0 software package provided by the manufacturer. The data from the first injection (1 μL) in each experiment was not used in the analysis. Four independent experiments were analyzed separately, and the fitted parameters were averaged. The heat capacity change (ΔC_p) associated with the binding of AVPI to XIAP-BIR3 was obtained from the temperature dependence of the calorimetric enthalpy (ΔH^{cal}) of binding, assuming linear behavior.

2.7. Differential scanning calorimetry (DSC)

DSC thermograms were obtained using a VP-DSC from MicroCal, Llc. (Northampton, MA). XIAP-BIR3 (50 μM) was prepared in 15 mM Tris, 150 mM NaCl and 1 mM DTT (pH 7.4) in the absence or presence of AVPI (150 μM). The reference cell was filled with the same buffer used for sample preparation. To prevent the formation of air bubbles, the samples and buffers were degassed exhaustively before filling the calorimeter cells. In this case, the unfolding process was irreversible due to protein aggregation, and we were able to obtain only the calorimetric enthalpy. Scan rate dependence was observed, where slow scan rates favored protein aggregation. A scan rate of 90 °C h^{-1} was used for all experiments to avoid any baseline anomalies due to protein precipitation.

2.8. Nuclear magnetic resonance (NMR)

^{1}H-^{15} N heteronuclear single quantum coherence spectra (HSQC) and heteronuclear Nuclear Overhauser effect (NOE) measurements were acquired at 15 °C at 600 MHz in a Bruker DRX600 spectrometer (Bruker Biospin GmbH, Rheinstetten, Germany) using a 5-mm cryogenic inverse-detection triple-resonance probe with a z gradient (TCI, Bruker Biospin GmbH, Rheinstetten, Germany). The proteins were dialyzed and concentrated in 15 mM Tris, 150 mM NaCl, and 1 mM DTT, pH 7.4. Samples were prepared with 10% D_2O (Isotec, Miamisburg, OH). The NMR data were processed with NMRpipe [40] and analyzed using NMRVIEW, version 5.0.3 [41]. The ^{1}H-^{15} N HSQC spectra of the XIAP-BIR3 were assigned according to Sun et al. [11].

2.9. Molecular dynamics simulations (MDS)

GROMACS is a software suite that is used to generate and analyze MD simulations [42]. Using GROMACS version 4, we ran 50-ns simulations of both systems to generate structural diversity for each protein set. One of the systems examined was the XIAP-BIR3 protein (with 115 residues) complexed with a zinc ion and the other used the first system, but complexed with the tetrapeptide, AVPI. Each system additionally consisted of the following: an edge of 9.0 nm at the simulation box fulfilled with simple point charge [43] water molecules and one sodium ion for system charge neutralization, giving approximately 72,000 atoms in the system. Each system, treated with a periodic boundary condition, underwent a 5000-step energy minimization using the steepest descent algorithm, while restraining the heavy atoms in the system. This was followed by a 5000-step energy minimization using the steepest descent algorithm without any restriction on the atoms. Another 5000-step energy minimization was carried out while applying a conjugated gradient algorithm. Thus, a 1-ns harmonic position restrained the MD simulation at 288 K, at which temperature all the protein atoms remained motionless. The electrostatic, the neighbor list switch and van der Waals interactions were set to 1.1, 1.1 and 0.9 nm, respectively. We used separate external temperature baths [44] at 288 K and a coupling constant $tau_T = 0.1$ ps for the protein and non-protein components of each system. The 20-ns production run simulation was carried out at constant pressure of 1 bar, and this pressure was maintained by coupling the system weakly to pressure baths [44] using $tau_P = 1.0$ ps and a constant temperature, as above. An integration time step of 2 fs was used with the LINCS [45] algorithm, constraining all covalent bonds to their equilibrium lengths. The force field used was GROMOS96 [46], 53a6. For each system, a structural ensemble was created by extracting structures generated by the simulation every 2.0 ps.

3. Results

3.1. Characterization of the interaction between XIAP-BIR3 and AVPI

We used isothermal titration calorimetry (ITC) to study the interaction between XIAP-BIR3 and AVPI, allowing the thermodynamic ligand-binding parameters to be determined with accuracy [47]. Fig. 1A depicts a representative experiment, showing the determination of the exothermic heat of binding from successive injections of AVPI into the cell containing BIR3 at 25 °C, after correction for the heat of dilution of AVPI. The discontinuity in the heat flux profile is due to differences in the injection volume, as indicated by the arrow. The peaks show a decrease in area after each ligand addition until saturation is achieved. The enthalpy changes at 25 °C as a function of the concentration of AVPI are shown in Fig. 1B. Our results show that the binding of AVPI to XIAP-BIR3 occurs in equimolar proportion ($n \sim 1$). The binding is exothermically and entropically favored in the temperature range studied (Table 1). The binding constant and the Gibbs free energy change were also obtained from the ITC data (Table 1). Changes in heat capacity can be used to estimate the thermodynamic contribution of bound waters in protein complexes [48]. In our study, we calculated the heat capacity change (ΔC_p) of the binding from the linear dependence of the binding enthalpy on temperature. A negative heat capacity ($\Delta C_p = -157.3$ cal mol^{-1} K^{-1}) was observed for the XIAP-BIR3/AVPI interaction.

The intrinsic fluorescence of tryptophan provides a convenient means of monitoring conformational changes in proteins, as it is sensitive to the polarity of the environment. The XIAP-BIR3 domain

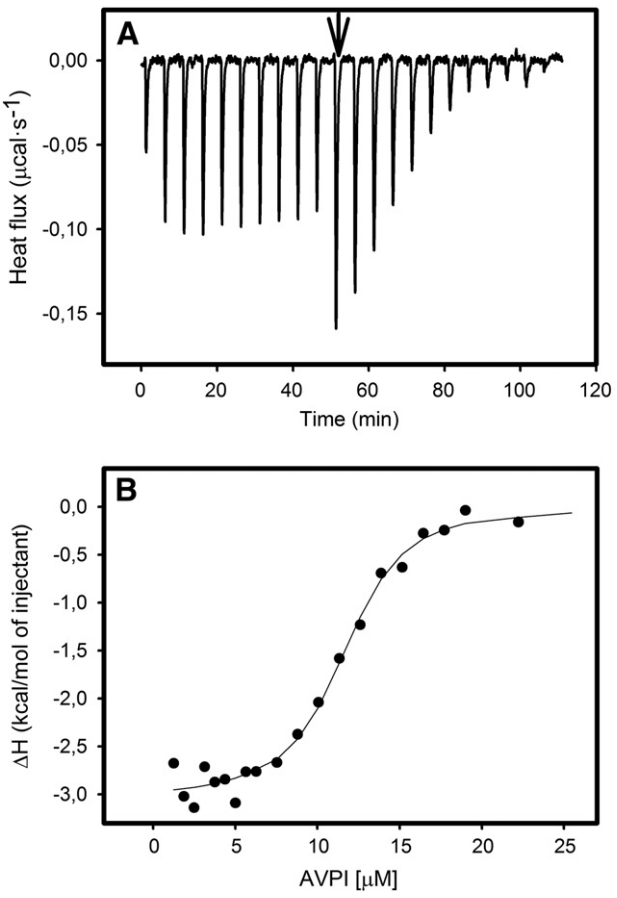

Fig. 1. Calorimetric titration of XIAP-BIR3 with AVPI. (A) The heat flux profile associated with the injections of the ligand to the calorimetric cell at 25 °C. The arrow indicates where the volume of titration was increased. (B) The binding isotherm at 25 °C. The measurements were also carried out at 10 and 37 °C.

Table 1
Binding parameters for the XIAP-BIR3/AVPI interaction estimated from ITC data.

Parameter	Temperature		
	10 °C	25 °C	37 °C
n	1.1 ± 0.1	1.1 ± 0.1	1.1 ± 0.1
K ($10^6 M^{-1}$)	4.2 ± 0.9	7.8 ± 1.2	8.5 ± 0.4
ΔH (kcal · mol^{-1})	−1.2 ± 0.1	−3.1 ± 0.1	−5.5 ± 0.1
ΔS (cal · $mol^{-1} \cdot K^{-1}$)	26.6 ± 0.8	19.1 ± 1.3	10.7 ± 0.7
ΔG (kcal · mol^{-1})	−8.5	−8.8	−8.9

The data are the mean values of three independent experiments ± the standard deviation.

has four tryptophan residues. Two of these, W310 and W323, are partially exposed to the solvent and interact with AVPI on formation of the complex [14]. Here these residues were used to follow the binding of AVPI to XIAP-BIR3 using fluorescence spectroscopy. The interaction between XIAP-BIR3 and AVPI was investigated by monitoring the intensity of the intrinsic fluorescence emission spectra and the center of spectral mass as the concentration of AVPI was increased from 2 to 60 μM (Fig. 2A, B). The spectral center of mass increased gradually as the ligand:domain molar ratio was raised, reaching a maximum at saturating concentrations (i.e., at a 3:1 ligand: domain molar ratio). These data show that the environment of Trp changes during the interaction and confirm the contact made between AVPI and these residues. Thus, we carried out all stability studies using a 3:1 AVPI:XIAP-BIR3 molar ratio.

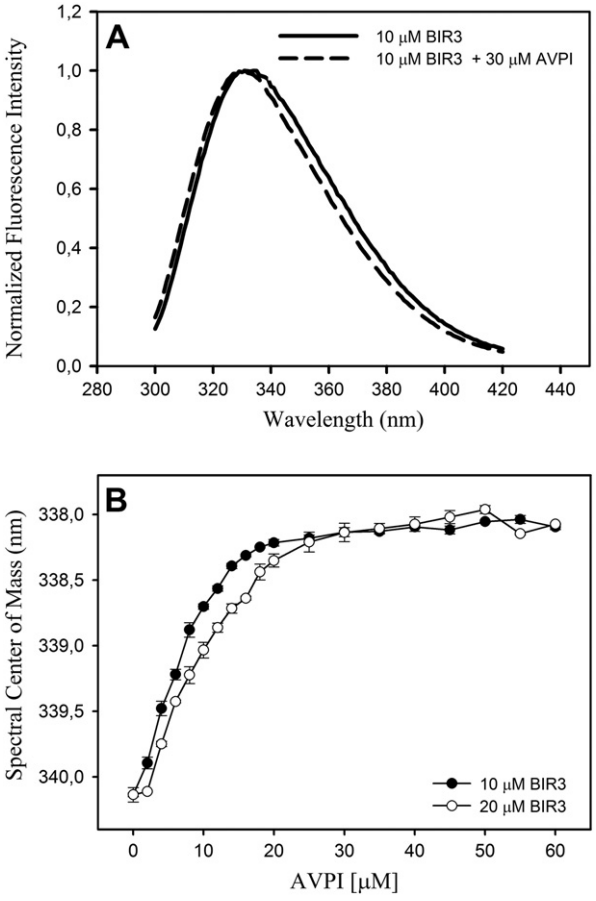

Fig. 2. Fluorescence analysis of XIAP-BIR3 and the AVPI interaction complex. (A) Normalized fluorescence spectra of the XIAP-BIR3 domain and the XIAP-BIR3/AVPI complex. (B) The spectral center of mass changes after the concentration of the tetrapeptide is increased. Buffer: 10 mM Tris, 150 mM NaCl and 1 mM DTT, pH 7.4.

3.2. The binding of AVPI induces an increase in the stability of XIAP-BIR3 toward chemical agents

Urea and guanidine hydrochloride are potent denaturants, which destabilize the secondary and tertiary structures of proteins by disrupting the hydrogen bonds and hydrophobic and electrostatic interactions. To measure the stability of XIAP-BIR3, which consists of five α-helices and a three-stranded β-sheet [11], we used fluorescence and CD with increasing concentrations of urea (0.5 to 9.3 M) or guanidine hydrochloride (data not shown). The samples were incubated overnight at each concentration of urea. Because tryptophan fluorescence spectra are sensitive to the environment, the unfolding of XIAP-BIR3 could be followed by measuring the red shift of the fluorescence spectra by decreases of the spectral center of mass. We also monitored changes in the secondary structure (by CD analysis at 228 nm) induced by treatment with urea at each denaturant concentration. To analyze these results more thoroughly, we converted the data to unfolded fraction values (Fig. 3A). The XIAP-BIR3 domain was very stable toward urea, as an increase of the unfolded fraction was only observed at 6 M urea (Fig. 3A). The same measurements were performed in the presence of the tetrapeptide to determine if the changes in the stability of XIAP-BIR3 are promoted by AVPI binding. The results showed that AVPI increases the stability of the XIAP-BIR3 domain towards urea. This stabilization can also be observed by

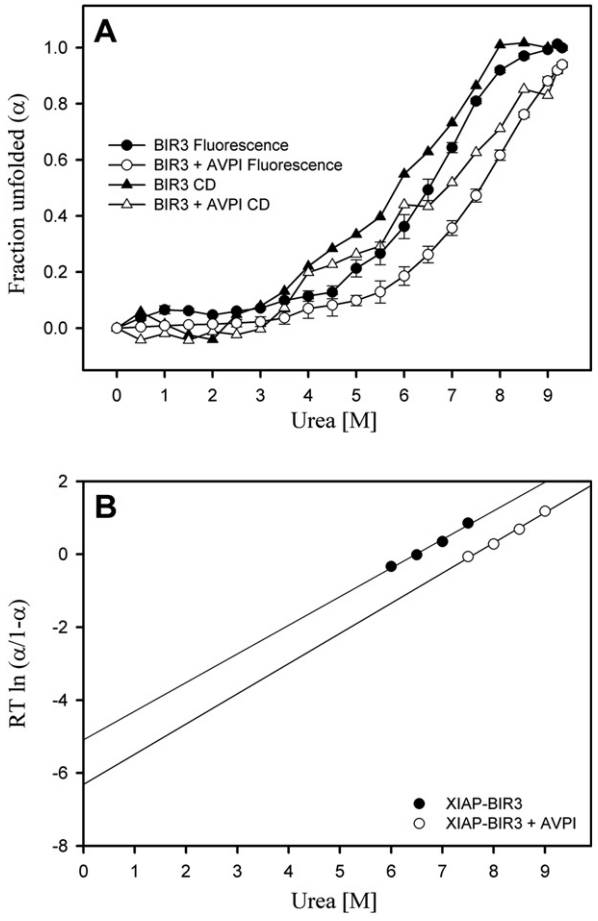

Fig. 3. The conformational stability of the XIAP-BIR3 domain towards urea. (A) The BIR3 domain and the BIR3-AVPI complex were incubated overnight at room temperature in the presence of the indicated concentrations of urea. To analyze the tertiary structure, we monitored the spectral center of mass changes in the fluorescence data. The secondary structure was investigated using the raw ellipticity at 228 nm for the urea experiments. (B) A plot of RT $\ln[\alpha/(1-\alpha)]$ *versus* urea concentration. The protein and AVPI concentrations used were 10 μM and 30 μM, respectively.

comparing the $[U]_{1/2}$ and $\Delta G°$ values in the absence and presence of AVPI (Fig. 3B and Table 2). After dilution of the unfolded sample to subdenaturing concentrations or the removal of urea by dialysis, we verified that the spectral center of mass and the ellipticity return to a value close to the initial one (data not shown). Thus, XIAP-BIR3 unfolding was fully reversible in the absence and presence of AVPI under these conditions.

3.3. The XIAP-BIR3-AVPI complex is highly stable and not dissociable by pressure

Studies on the effects of high pressure on biological systems have provided new information on protein–protein, protein–ligand, and protein–nucleic acid interactions and on virus assembly [49,50]. In addition, pressure is a physical agent and, like temperature, it is relevant in the study of protein unfolding and protein–protein interactions. The advantage of using hydrostatic pressure or temperature to study protein stability is that they induce less drastic changes than do chemical agents. Hence, these methods do not represent a chemical interference with the sample [50]. For this reason, we also investigated the effects of high pressure and temperature on the stability of XIAP-BIR3. After increasing the pressure to 3 kbar, the spectral center of mass was not significantly affected. This result confirms that XIAP-BIR3 is quite stable under high pressure (Fig. 4A). When XIAP-BIR3 was bound to AVPI, the complex remained stable, and the increase in pressure did not induce the dissociation of AVPI (Fig. 4A).

3.4. AVPI binding induces an increase in the thermal stability of the XIAP-BIR3 domain

Differential scanning calorimetry (DSC) has been widely used to study folding and unfolding processes in proteins. In this work, we used DSC to investigate the thermal stability of XIAP-BIR3 and the effects of AVPI binding. Fig. 4B shows the experimental thermograms for the free XIAP-BIR3 domain and for XIAP-BIR3 in the presence of AVPI.

The thermogram of free XIAP-BIR3 shows a single peak for the thermally induced unfolding process, with the denaturation temperature (T_m) equal to 68.9 °C and a calorimetric enthalpy (ΔH^{cal}) change of 25.6 kcal mol^{-1} (Fig. 4B and Table 2). At a ligand:protein molar ratio of 3:1, AVPI binding increases the thermal stability of XIAP-BIR3 considerably, as observed by the increases in both the T_m and the calorimetric enthalpy (Fig. 4B). Upon AVPI binding, the T_m of XIAP-BIR3 increased by 8.4 °C and the ΔH^{cal} increased by 58.7 kcal mol^{-1} (Table 2). These data confirm that the stability of XIAP-BIR3 increases after AVPI binding, as observed by fluorescence and CD using urea-induced denaturation. We were not able to obtain the unfolding enthalpy due to protein aggregation.

Table 2
Thermodynamic parameters of the unfolding of the XIAP-BIR3 domain in the absence and presence of AVPI.

	T_m(°C)	Q/mol $_{(Tm)}$ (kcal/mol)	$U_{1/2}$ Fluor (M)	$U_{1/2}$ CD (M)	$\Delta G°_{25\ °C}$ (kcal/mol)
XIAP-BIR3	68.9 ± 0.1	25.7 ± 2.2	6.5	5.8	5.1
XIAP-BIR3/AVPI	77.3 ± 0.1	84.4 ± 3.4	7.6	6.9	6.2

The enthalpy values were obtained from differential scanning calorimetry analysis. The Q/mol (the heat released per mol) utilized was measured at the T_m at which the ΔG is zero. $[U]_{1/2}$ corresponds to the concentrations of urea that cause 50% denaturation of the XIAP-BIR3 domain as verified using fluorescence (Fluor) and circular dichroism (CD). The Gibbs free energies ($\Delta G°$) were calculated from the urea denaturation data using Eq. (2).

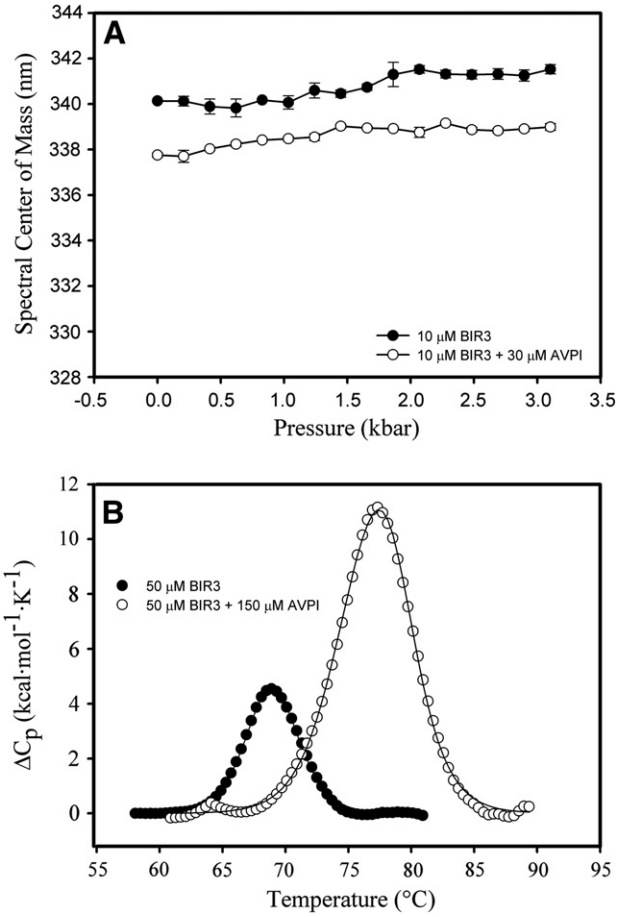

Fig. 4. The conformational stability of the XIAP-BIR3 domain towards physical agents. (A) At room temperature, significant changes in the XIAP-BIR3 structure were not promoted at pressures below 3.1 kbar. The incubation time at each pressure was 10 min. All data points represent the average and standard deviation of three experiments. The protein concentration was 10 μM. (B) Thermal unfolding curves of XIAP-BIR3 in the presence and absence of AVPI. The experimental thermograms of XIAP-BIR3 are shown in the absence (closed circles) and in the presence (open circles) of AVPI after baseline subtraction. In both cases, the solid line represents the best fit. For all DSC experiments, the protein concentration was 50 μM, and the AVPI concentration was 150 μM.

3.5. The effects of AVPI on the secondary structure of XIAP-BIR3

To investigate possible changes in the secondary structure that could be associated with stabilization of the XIAP-BIR3 domain, we used circular dichroism (CD). Although this domain also contains β-strand structures [11], the CD spectrum of XIAP-BIR3 is characteristic of α-helical structures, with ellipticity minima at 209 and 224 nm. The binding of AVPI promoted alterations in the rotation of circularly polarized light at 210–225 nm, suggesting slight changes in the secondary structure (Fig. 5A).

To understand the effects of AVPI binding on the structure and dynamics of XIAP-BIR3 more thoroughly, we also used NMR and molecular dynamics simulations in the absence and presence of AVPI. In our molecular dynamics simulations, the root mean square deviation (RSMD) measurements of the backbone atoms of XIAP-BIR3 and of the XIAP-BIR3/AVPI complex show that the system is stabilized after 10 ns (Fig. 7A). The changes observed in the CD spectra (Fig. 5A) and, in particular, the molecular dynamics simulations suggest that in the presence of AVPI, there is a stabilization of hydrogen bonds (Fig. 5B) and of different secondary structures, mainly β-strands (Fig. 5C).

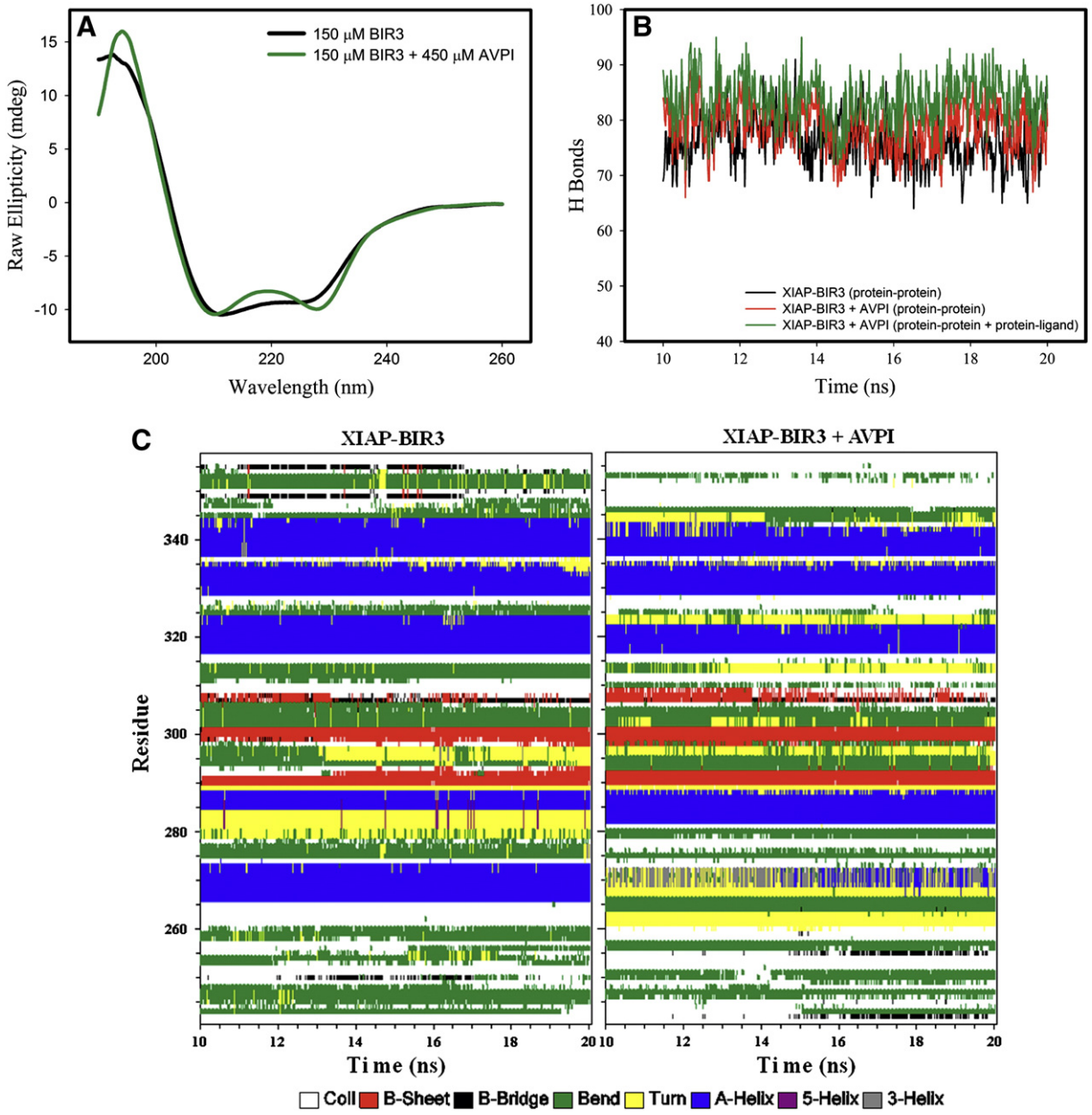

Fig. 5. The secondary structures of the XIAP-BIR3 domain and the XIAP-BIR3/AVPI complex, as verified by circular dichroism and molecular dynamics simulations. (A) CD spectra of the XIAP-BIR3 domain and the XIAP-BIR3/AVPI complex. The concentration of the domain was 150 μM. (B) The hydrogen-bonding profiles of the XIAP-BIR3 domain and the XIAP-BIR3/AVPI complex during the simulation period between 10 and 20 ns. (C) The types of secondary structure are color-coded as noted in the figure. The simulations were generated from structures deposited in the PDB. PDB ID: 1f9x (the XIAP-BIR3 domain) and 1g3f (the XIAP-BIR3/AVPI complex) [11,14].

3.6. The effects of AVPI on the dynamics of XIAP-BIR3

From our analysis of the domain dynamics using NMR, we can verify that several resonances of XIAP-BIR3 are missing in the HSQC spectrum in the absence of the peptide (Fig. 6A, in red), and this is typical of conformational exchange occurring on a timescale of milli- to microseconds. Extensive line broadening occurs when the conformational switch is the intermediate exchange regime, i.e., the rate of exchange is approximately the chemical shift difference between each conformational sub-state ($k_{ex} \sim \Delta\nu$). The residues involved in conformational exchange are from the N- and C-terminal regions and in two loops (residues 276–280 and 308–314) [14]. In other words, these residues have two or more conformational sub-states. The type of motion means that the energy barriers for inter-conversion among these sub-states are higher than the thermal energy (kT) [51].

Upon addition of AVPI, several new resonances appear as sharp lines in the spectra (Fig. 6A, in black). This is a strong indication that AVPI leads to stabilization of one of the conformational sub-states. This is the so-called conformational selection mechanism of binding [51]. Once AVPI is bound, the energy of this conformational sub-state is lowered and there is a population shift toward the lowest energy state. In addition, the new resonances that appear in the HSQC spectrum of the XIAP-BIR3/AVPI complex due to conformational selection do not exhibit decreased heteronuclear NOEs, indicating that the residues corresponding to these resonances are rigid in the bound state (Fig. 6C, in black). This validates and corroborates the molecular dynamics simulation data (i.e., the RMSF, Fig. 7B). Loop (293–299), however, displays negative (in red) or near zero (black- or green-dashed circles) heteronuclear NOEs (Fig. 6B, C), indicating local thermal motions that occur on a fast time scale with respect to molecular tumbling, also corroborating

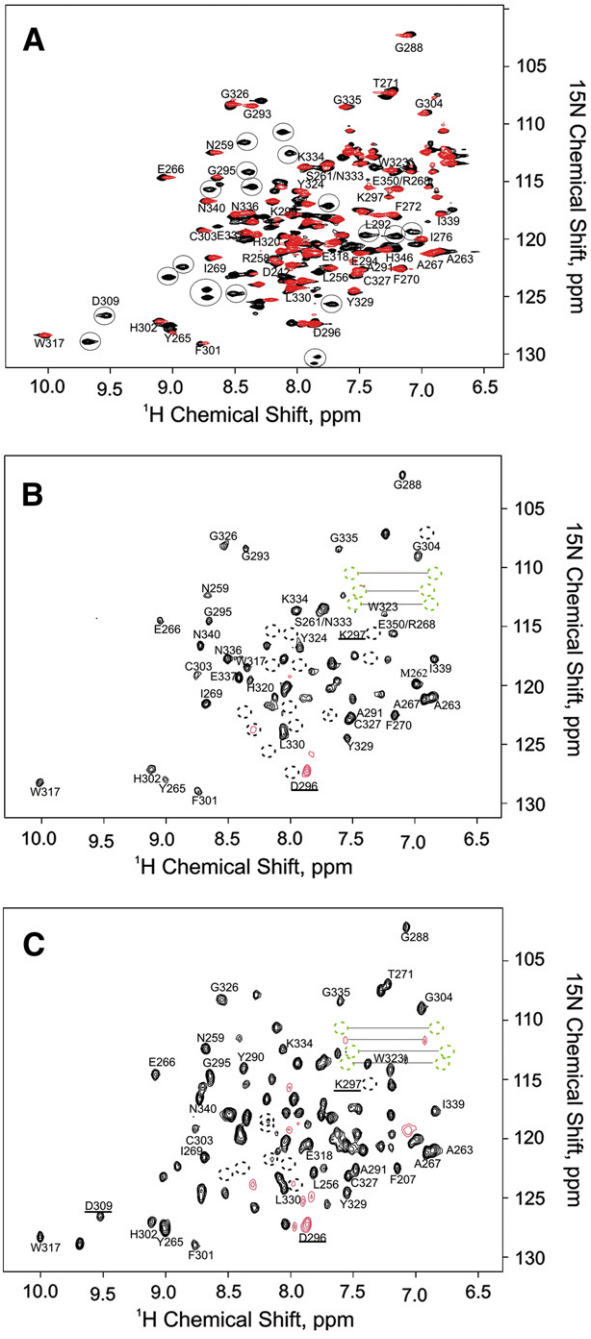

Fig. 6. Analysis of the XIAP-BIR3/AVPI interaction using nuclear magnetic resonance. (A) ^{1}H-^{15} N HSQC spectrum of the XIAP-BIR3/AVPI complex (in black) superimposed on the XIAP-BIR3 free domain (in red) showing the appearance of new peaks (highlighted in black circles) that were not observed for the free protein at 15 °C. (B) and (C) ^{1}H-^{15} N Heteronuclear NOEs of the free XIAP-BIR3 domain and the XIAP-BIR3/AVPI complex at 15 °C, respectively. The regions in fast thermal dynamics, where the heteronuclear NOEs are negative or close to zero are shown in red (negative peaks) or highlighted by dashed circles (the peak is absent because the NOEs are close to zero). Backbone residues are shown in black dashed circles, whereas the side chains of glutamine and asparagine are shown in green dashed circles. Residues D309 (representing loop (309–314)), which is rigid after AVPI binding, and D296/K297 (representing loop (293–299), which remain flexible, are underlined.

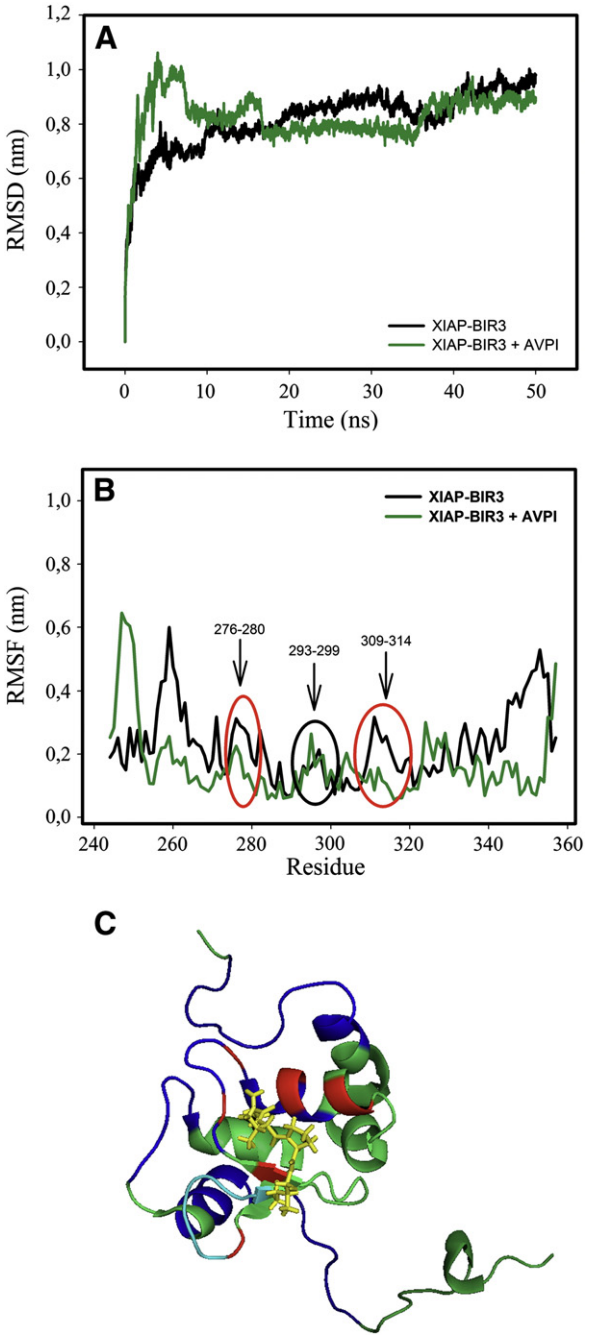

Fig. 7. Molecular dynamics simulations reveal the effects of AVPI binding on the dynamics of the XIAP-BIR3 domain. (A) Root Mean Square Deviations (RSMDs) of the backbone atoms of XIAP-BIR3 and the XIAP-BIR3/AVPI complex. (B) Root-mean-square fluctuations (RMSFs) of the XIAP-BIR3 domain and the changes promoted by the binding of AVPI. The loops that have been stabilized are surrounded in red, and the loop that has not been stabilized is surrounded in black. (C) Structure of XIAP-BIR3/AVPI complex (PDB ID: 1g3f). The residues of the XIAP-BIR3 domain involved in the interaction with AVPI are colored in red, and the loops and terminal regions that are stabilized are represented in blue. The tetrapeptide AVPI is represented in yellow and the loop that has not been stabilized is represented in cyan.

the molecular dynamic simulations data. These results confirm that the selection of some conformer(s) in solution involves dynamic restriction of loop (276–280), loop (309–314) and the N- and C-terminal regions and that loop (293–299) remains highly flexible in the complex.

Adding structural details and corroborating the NMR results, the root-mean-square fluctuations (RSMF) measurements showed that the flexibility of the same loops (residues 276–280 and 308–314) is reduced in the presence of AVPI, including loop (276–280), which forms the binding site (Fig. 7B, C). The terminal regions that are highly flexible in the free protein are also stabilized by AVPI binding (Fig. 7B,

C). Loop (293–299) remains flexible, as verified also by the NMR data. All these results strongly indicate that AVPI binding promotes a large loss of conformational entropy.

4. Discussion

In recent years, the structures of many apoptotic proteins have been solved by X-ray crystallography and NMR and used in drug design [52]. However, despite the extensive knowledge of their structures, the mechanisms and thermodynamic stabilities of the interactions of these proteins with cellular targets are still poorly understood.

The XIAP-BIR3 domain is of particular interest because it is a promising target in cancer therapy. Its inhibition allows tumorigenic cells that overexpress XIAP to enter into apoptosis [53,54]. Recent studies have shown that overexpression of XIAP in some carcinomas predicts worse prognoses [21] and play an important role in the regulation of the apoptotic responses in cancer cells to both immune- and drug-mediated therapies [23,24,27,29]. In addition, downregulation or inhibition of XIAP may reverse immune and therapy resistance [23,27]. During apoptosis, the IAP-mediated inhibition of caspase is removed by the mitochondrial protein known as Smac or DIABLO [13,55], mainly by the interaction between the XIAP-BIR3 domain and the AVPI tetrapeptide from Smac [14]. Previous studies have shown that Smac peptides in the cytosol potentiate the tumor-suppressive activity of the chemotherapeutic agent *in vitro* and *in vivo* with minimal toxicity [29]. Many studies have attempted to explore this interaction [14,27] and to develop drugs that bind to IAPs promoting its inhibition [27–30]. The 3D structure of the complex between XIAP-BIR3 and AVPI-Smac is available [14]. Understanding the dynamics and stability of this complex and characterizing the AVPI-binding parameters will improve our understanding of the XIAP-BIR3 inhibition and may help in the development of new strategies for cancer treatment.

A fully thermodynamic evaluation (in terms of the enthalpy and entropy components apart from the heat capacity variation) of the interaction between AVPI and XIAP-BIR3 was carried out here to assist the understanding of XIAP-BIR3 inhibition. To design more efficient drugs, it is crucial to correlate the thermodynamic and structural data [35,56–58]. Our data show that the XIAP-BIR3/AVPI interaction is both enthalpically and entropically favored (Table 1) and has a negative variation in the heat capacity ($\Delta C_p = -157.13$ cal mol^{-1} K^{-1}). Changes in heat capacity are not restricted to the interactions between non-polar groups in water [48]. However, the fact that the binding is entropically driven (Table 1), even with a loss of conformational entropy (Figs. 6 and 7), indicates that hydrophobic interactions play an important role in both the interaction and protein stabilization. Thus, we can conclude that desolvation of the ligand and the binding site is driven mainly by the enhanced entropy of water, a key-step in the binding of AVPI to XIAP-BIR3.

Protein thermal stability is modified by ligand binding due to the coupling between two mutual processes under equilibrium: binding and unfolding [59–62]. Additional binding free energy is responsible for shifting the unfolding temperature, and it may or may not include contributions from conformational changes. Information about changes in structure and flexibility associated with molecular recognition is important to understanding the thermodynamics of interaction and for drug discovery. Here we show that the binding of the AVPI tetrapeptide leads to stabilization of BIR3 against urea- and temperature-induced unfolding (Table 2). However, it is important to understand whether this stabilization results from changes in the conformation of XIAP-BIR3. The small change in the CD spectra (Fig. 5A) could be related to the formation of a short anti-parallel β-strand within the three-stranded β-sheet of XIAP-BIR3 upon AVPI binding [15], but it could also be due to stabilization of one or more pre-existent conformational states, as verified by NMR analyses (Fig. 6A). In addition, our molecular dynamics simulations of the XIAP domain and the XIAP-BIR3/AVPI complex (Fig. 5C) indicate that β-strand structures are stabilized due to AVPI binding. Thus, the binding of AVPI appears to select more rigid conformer(s) and with more stable β-strand structures.

The two principal forces that stabilize protein structure are the hydrophobic effect and hydrogen bonding, and the main destabilizing force is the loss of conformational entropy [63]. Molecular dynamics simulations indicate that the network of hydrogen bonds in XIAP-BIR3 is slightly stabilized by AVPI (Fig. 5B), and some of these likely involve β-strands (Fig. 5C). By measuring the H-bond coupling constants using NMR, other authors have also shown that the binding of ligands can affect protein hydrogen-bonding networks [64]. For instance, ligand binding to the SH3 domain induces strain in the hydrogen bonds that buttress the SH3/ligand binding surface, and small changes in the lengths of hydrogen bonds are propagated throughout the domain. Thus, the high increase in the heat involved in XIAP-BIR3 denaturation is due to the positive variation in the heat capacity of unfolding (Fig. 4B and Table 2). However, there may also be a contribution from the hydrogen bond stabilization that is promoted by AVPI binding.

Changes in flexibility upon ligand binding, mutation, or changes in sample conditions can be interpreted in terms of contributions to conformational entropy. Backbone and side chain flexibility can either decrease or increase upon ligand binding [65]. Decreases are often associated with “enthalpy–entropy compensation” and “induced fit or conformational selection” binding, whereas increases in conformational entropy can contribute to the stabilization of complexes. Liu et al. [14] observed that two loops of the XIAP-BIR3 domain, which could not be structurally characterized by NMR in the free protein, became well defined upon AVPI binding. Remarkably, a single mutation (G306E) that stabilizes these loops promotes changes in ligand affinity [66]. In this case, there is a loss of favored entropy in the interaction that is related to the reduction of hydrophobic contacts. Our molecular dynamics simulations of the domain and the complex (Fig. 7) also suggested that the binding of AVPI reduces the conformational flexibility of loop (276–280) and loop (309–314) of the domain (Fig. 7B, C), in which the loop (309–314) is involved in the interaction. The free XIAP-BIR3 domain presents highly disordered and flexible N- and C-terminals as verified by molecular dynamics simulations (Fig. 7B), and these domains are stabilized by AVPI binding (Fig. 7B, C). Heteronuclear NOE data corroborate the stabilization of the XIAP-BIR3 domain on the ns-ps timescale (Fig. 6C). All these data indicate a significant loss of conformational entropy in the XIAP-BIR3 domain associated with AVPI binding. Variations in the conformational entropy and heat capacity may both be important in stabilizing the folded structures of proteins [65] and are also important in the stabilization of XIAP-BIR3.

It is well known from fundamental thermodynamics that changes in flexibility upon binding modulate conformational entropy and that this contributes significantly to ΔC_p [67]. Both ps–ns and μs–ms timescale fluctuations, which can be probed by relaxation experiments, affect ΔC_p. Furthermore, restrictions of soft vibrational modes characterized by force constants weak enough to be affected by ligand binding have been suggested to account for up to 20% of the total ΔC_p [67]. Moreover, the redistribution of the native state ensemble induced by ligand binding appears to be a significant source of ΔC_p. A reduction of the population/density of microstates will contribute to an increased negative ΔC_p [68,69]. Our results show that binding of the peptide involves a conformational selection process (Fig. 6A) with a reduction in domain flexibility (Figs. 6 and 7). Therefore, our calorimetric data, which show a negative ΔC_p (-157.3 cal mol^{-1} K^{-1}) upon AVPI binding, appear to be strongly associated with protein dynamics, in addition to the contribution from hydrophobic interactions. It is interesting to note that even when hydrophobic interactions predominate (AVPI is hydrophobic), the decrease in conformational entropy is important for the reduction of ΔC_p and the binding of hydrophobic solutes. The number of conformers of the XIAP-BIR3/AVPI complex is most probably smaller than that for the free protein, resulting in a decrease in the entropic component of the free energy upon AVPI

binding. Therefore, the interaction between XIAP-BIR3 and AVPI is significantly compromised by the entropic free energy component, restricting the number of conformers.

The structural rigidity and flexibility of proteins are critically balanced after folding, and the binding of ligands may perturb the interplay between the entropic and enthalpic energetic contributions [70]. In the presence of optimal geometrical complementarity of the interacting species, the residual restriction of protein flexibility on ligand binding could dictate unfavorable conditions for the stability of the complex. An extensive exchange between enthalpy and entropy has been indicated for protein–protein interactions [71]. The conformational Gibbs energy (ΔG_{conf}) changes that were obtained from the urea denaturation experiments ($\Delta\Delta G = -1.1$ kcal mol^{-1}) show that XIAP-BIR3 is highly stabilized and that this stabilization is significantly important for AVPI affinity (Table 2). Although the variation in conformational entropy (ΔS_{conf}) is unfavorable (Figs. 6 and 7), the variation in binding entropy (ΔS_{bind}) is highly favorable (Table 1). Thus, it is likely that the high variation of hydration entropy (ΔS_{hydr}) associated with the hydrophobic contacts is essential for binding affinity and stabilization, indicating that the negative variation of heat capacity that occurs on binding to AVPI is also strongly associated with the hydrophobic effect. In conclusion, although the hydrogen bonds are also stabilized and involve dynamic restriction, our data strongly suggest that stabilization of the XIAP-BIR3 domain by the tetrapeptide AVPI is also strongly favored by hydrophobic factors.

While the enthalpy–entropy compensation is critical for the optimization of affinity [35,57], most drug-design strategies focus solely on promoting favorable intermolecular interactions. However, protein–drug associations often entail an entropic penalty, generally arising from induced fit, compromising the affinity. Recently, studies using NMR relaxation methods showed that when different peptides bind to calmodulin, the apparent change in the corresponding conformational entropy is linearly related to the change in overall binding entropy [72]. These results show that changes in the protein conformational entropy can significantly contribute to the free energy of protein-ligand association. In addition, other authors have demonstrated that induced disorder in protein–ligand complexes can provide an interesting drug-design strategy [73]. The loss of conformational entropy of the XIAP-BIR3 domain, which arises from conformational selection and from reduced flexibility (mainly from the two loops and the terminal regions that are related to binding), is a crucial unfavorable factor for the affinity of AVPI and appears to be an important aspect that can be manipulated in drug design procedures.

In summary, this study provides the first thermodynamic analysis of the unfolding of the XIAP-BIR3 domain and the XIAP-BIR3/AVPI complex. The simple model of XIAP-BIR3 interacting with AVPI that we have used in the present work is interesting because it addresses correlations among the changes in protein stability promoted by ligand interaction and the conformational selection process, dynamic restriction and the hydrophobic effect. We verified that the stabilization of the XIAP-BIR3 domain by interaction with AVPI results from the hydrophobic effect (entropy driven) and the stabilization of hydrogen bonds (enthalpy driven). These are partially compensated by a loss of conformational entropy, which is associated with the selection of pre-existent conformer(s) (on the ms–μs timescale) and a reduction in flexibility (on the ns–ps timescale). These data provide important additional information on the interaction between Smac/DIABLO and IAPs and help in understanding the nature of XIAP-BIR3 inhibition. This information may prove important in the design of anti-cancer drugs.

Acknowledgements

We are grateful to Emerson R. Gonçalves for the excellent technical assistance. We also would like to thank Dr. Yigong Shi for kindly providing the plasmid with the XIAP-BIR3 sequence.

This work was supported in part by an International Grant from ICGEB to J.L.S., by grants from the Millennium Institute for Structural Biology in Biomedicine and Biotechnology (CNPq Millennium Program), Fundação Carlos Chagas Filho de Amparo à Pesquisa do Estado do Rio de Janeiro (FAPERJ), Fundação Universitária José Bonifácio (FUJB), Conselho Nacional de Desenvolvimento Científico e Tecnológico (CNPq), and Pronex Program/CNPq of Brazil to J.L.S. and A.C.O., and by FINEP to M.L.B.

References

[1] H. Steller, Mechanisms and genes of cellular suicide, Science 267 (1995) 1445–1449.
[2] G.S. Salvesen, C.S. Duckett, IAPs proteins: blocking the road to death's door, Nat. Rev. Mol. Cell Biol. 3 (2002) 401–410.
[3] M. JacobsonWeil, M. Raff, Programmed cell death in animal development, Cell 88 (1997) 347–354.
[4] Q.L. Deveraux, J.C. Reed, IAP family proteins-supressors of apoptosis, Genes Dev. 13 (1999) 239–252.
[5] S.W. Fesik, Insights into programmed cell death through structural biology, Cell 103 (2000) 273–282.
[6] R. Takahashi, Q. Deveraux, I. Tamm, K. Welsh, N. Assa-Munt, G.S. Salvesen, J.C. Reed, A single BIR domain of XIAP sufficient for inhibiting caspases, J. Biol. Chem. 273 (1998) 7787–7790.
[7] S.J. Riedl, M. Renatus, R. Schwarzenbacher, Q. Zhou, C. Sun, S.W. Fesik, R.C. Liddington, G.S. Salvesen, Structural basis for the inhibition of caspase-3 by XIAP, Cell 104 (2001) 791–800.
[8] J. Chai, E. Shiozaki, S.M. Srinivasula, Q. Wu, P. Datta, E.S. Alnemri, Y. Shi, Structural basis of caspase-7 inhibition by XIAP, Cell 104 (2001) 769–780.
[9] Y. Huang, Y.C. Park, R.L. Rich, D. Segal, D.G. Myszka, H. Wu, Structural basis of caspase inhibition by XIAP: differential roles of the linker versus the BIR domain, Cell 104 (2001) 781–790.
[10] Q.L. Deveraux, E.L.H.R. Stennicke, K. Welsh, G.S. Salvesen, J.C. Reed, Cleavage of human inhibitor of apoptosis protein XIAP results in fragments with distinct specificities for caspases, EMBO J. 18 (1999) 5242–5251.
[11] C. Sun, M. Cai, R.P. Meadows, N. Xu, A.H. Gunasekera, J. Herrmann, J.C. Wu, S.W. Fesik, NMR structure and mutagenesis of the third BIR domain of the inhibitor of apoptosis protein XIAP, J. Biol. Chem. 275 (2000) 33777–33781.
[12] S.M. Srinivasula, R. Hegde, A. Saleh, P. Datta, J.C. Shiozaki, R.A. Lee, P.D. Robbins, T. Fernandes-Alnemri, Y. Shi, E.S. Alnemri, A conserved XIAP-interaction motif in caspase-9 and Smac/DIABLO regulates caspase activity and apoptosis, Nature 410 (2001) 112–116.
[13] J. Chai, C. Du, J.W. Wu, S. Kyin, X. Wang, Y. Shi, Structural and biochemical basis of apoptotic activation by Smac/DIABLO, Nature 406 (2000) 855–862.
[14] Z. Liu, C. Sun, E.T. Olejniczak, R.P. Meadows, S.F. Betz, T. Oost, J. Herrmann, J.C. Wu, S.W. Fesik, Structural basis of binding of Smac/DIALBLO to the XIAP BIR3 domain, Nature 408 (2000) 1004–1008.
[15] G. Wu, J. Chai, T.L. Suber, J. Wu, C. Du, X. Wang, Y. Shi, Structural basis of IAP recognition by Smac/DIABLO, Nature 408 (2000) 1008–1012.
[16] S.M. Srinivasula, P. Datta, X.J. Fan, T. Fernandes-Alnemri, Z. Huang, E.S. Alnemri, Molecular determinants of the caspase-promoting activity of Smac/DIABLO and its role in the death receptor pathway, J. Biol. Chem. 275 (2000) 36152–36157.
[17] J.W. Wu, A.E. Cocina, J. Chai, B.A. Hay, Y. Shi, Structural analysis of a functional DIAP1 fragment bound to grim and hid peptides, Mol. Cell 8 (2001) 95–104.
[18] G. Ambrosini, C. Adida, D.C. Altieri, A novel anti-apoptosis gene, surviving, expressed in cancer and lymphoma, Nat. Med. 3 (1997) 917–921.
[19] L. Tamm, S.M. Kornblau, H. Segall, S. Krajewski, K. Welsh, S. Kitada, D.A. Scudiero, G. Tudor, Y.H. Qui, A. Monks, M. Andreeff, J.C. Reed, Expression and prognostic significance of IAP-family genes in human cancers and myeloid leukemias, Clin. Cancer Res. 6 (2000) 1796–1803.
[20] D. Vucic, H.R. Stennicke, M.T. Pisabarro, G.S. Salvesen, V.M. Dixit, ML-IAP, a novel inhibitor of apoptosis that is preferentially expressed in human melanomas, Curr. Biol. 10 (2000) 1359–1366.
[21] Y. Mizutani, H. Nakanishi, Y.N. Li, H. Matsubara, K. Yamamoto, N. Sato, T. Nakamura, K. Mikami, N. Takaha, O. Ukimura, A. Kawauchi, N. Nonomura, B. Bonavida, T. Miki, Overexpression of XIAP expression in renal cell carcinoma predicts a worse prognosis, Int. J. Oncol. 30 (4) (2007) 919–925.
[22] M. Holcik, C. Yeh, R.G. Korneluk, T. Chow, Translational upregulation of X-linked inhibitor of apoptosis (XIAP) increases resistance to radiation induced cell death, Oncogene 19 (2000) 4174–4177.
[23] H. Sasaki, Y. Sheng, F. Kotsuji, B.K. Tsang, Down-regulation of X-linked inhibitor of apoptosis protein induces apoptosis in chemoresistant human ovarian cancer cells, Cancer Res. 60 (2000) 5659–5666.
[24] C.P. Ng, B. Bonavida, X-linked inhibitor of apoptosis (XIAP) blocks Apo-2 ligand/tumor necrosis factor-related apoptosis-inducing ligand mediated apoptosis of prostate cancer cells in the presence of mitochondrial activation: sensitization by overexpression of second mitochondria-derived activator of caspase/direct IAP-binding protein with low pl (Smac/DIABLO), Mol. Cancer Ther. 1 (2002) 1051–1058.
[25] Y. Hu, G. Cherton-Horvat, V. Dragowska, S. Baird, R.G. Korneluk, J.P. Durkin, L.D. Mayer, E.C. LaCasse, Antisense oligonucleotides targeting XIAP induce apoptosis and enhance chemotherapeutic activity against human lung cells in vitro and in vivo, Clin. Cancer Res. 9 (2003) 2826–2836.

[26] Z. Nikolovska-Coleska, R. Wang, X. Fang, H. Pan, Y. Tomita, P. Li, P.P. Roller, K. Krajewski, N.G. Saito, J.A. Stuckey, S. Wang, Development and optimization of a binding assay for the XIAP BIR3 domain using fluorescence polarization, Anal. Biochem. 332 (2004) 261–273.
[27] T.K. Oost, C. Sun, R.C. Armstrong, A. Al-Assaad, S.F. Betz, T.L. Deckwerth, H. Ding, S.W. Elmore, R.P. Meadows, E.T. Olejniczak, A. Oleksijew, T. Oltersdorf, S.H. Rosenberg, A.R. Shoemaker, K.J. Tomaselli, H. Zou, S.W. Fesik, Discovery of potent antagonists of the antiapoptotic protein XIAP for the treatment of cancer, J. Med. Chem. 47 (2004) 4417–4426.
[28] S. Fulda, W. Wick, M. Weller, K.M. Debatin, Smac agonists sensitize for Apo2L/TRAIL- or anticancer drug-induced apoptosis and induce regression of malignant glioma in vivo, Nat. Med. 8 (2002) 808–815.
[29] C.R. Arnt, M.V. Chiorean, M.P. Heldebrant, G.J. Gores, S.H. Kaufmann, Synthetic Smac/DIABLO peptides enhance the effects of chemotherapeutic agents by binding XIAP and cIAP1 in situ, J. Biol. Chem. 277 (2002) 44236–44243.
[30] L. Yang, T. Mashima, S. Sato, M. Mochizuki, H. Sakamoto, T. Yamori, T. Oh-hara, T. Tsuruo, Predominant suppression of apoptosome by inhibitor of apoptosis protein in non-small cell lung cancer H460 cells: therapeutic effect of a novel polyarginine-conjugated Smac peptide, Cancer Res. 63 (2003) 831–837.
[31] H. Sun, J.A. Stuckey, Z. Nikolovska-coleska, D. Qin, J.L. Meagher, S. Qiu, J. Lu, C. Yang, N.G. Saito, S. Wang, Structure-based design, synthesis, evaluation, and crystallographic studies of conformationally constrained smac mimetics as inhibitors of the X-linked inhibitor of apoptosis protein (XIAP), J. Med. Chem. 51 (2008) 7169–7180.
[32] R.B. Gonçalves, D. Sanches, T.L. Souza, J.L. Silva, A.C. Oliveira, The proapoptotic protein Smac/DIABLO dimer has the highest stability as measured by pressure and urea denaturation, Biochemistry 47 (12) (2008) 3832–3841.
[33] S.M. Lima, A.C. Vaz, T.L. Souza, D.S. Peabody, J.L. Silva, A.C. Oliveira, Dissecting the role of protein-protein and protein-nucleic acid interactions in MS2 bacteriophage stability, FEBS J. 273 (7) (2006) 1463–1475.
[34] E. Freire, The thermodynamic linkage between protein structure, stability, and function, Methods Mol. Biol. 168 (2001) 37–68.
[35] T.S.G. Olsson, M.A. Williams, W.R. Pitt, J.E. Ladbury, The thermodynamics of protein–ligand interaction and solvation: insights for ligand design, J. Mol. Biol. 384 (2008) 1002–1017.
[36] E.A. Ribeiro Jr., C.H. Ramos, Circular permutation and deletion studies of myoglobin indicate that the correct position of its N-terminus is required for native stability and solubility but not for native-like heme binding and folding, Biochemistry 44 (2005) 4699–4709.
[37] I. Cherny, M. Overgaard, J. Borch, Y. Bram, K. Gerdes, E. Gazit, Structural and thermodynamic characterization of the *Escherichia coli* RelBE toxin–antitoxin system: indication for a functional role of differential stability, Biochemistry 46 (43) (2007) 12152–12163.
[38] N.C. Pace, Determination and analysis of urea and guanidine hydrochloride denaturation curves, Methods Enzymol. 131 (1986) 266–280.
[39] G. Weber, Protein interactions, Chapman and Hall, New York, 1992.
[40] F. Delaglio, S. Grzesiek, G.W. Vuister, G. Zhu, J. Pfeifer, A. Bax, NMRPipe: a multidimensional spectral processing system based on UNIX pipes, J. Biomol. NMR 6 (3) (1995) 277–293.
[41] B.A. Johnson, R.A. Blevins, NMRView: a computer program for the visualization and analysis of NMR data, J. Biomol. NMR 4 (1994) 603–614.
[42] L.B. Hess, C. Kutzner, D. van der Spoel, E. Lindahl, GROMACS 4: algorithms for highly efficient, load-balanced, and scalable molecular simulation, J. Chem. Theory Comput. 4 (2) (2008) 435–447.
[43] H.J.C. Berendsen, J.P.M. Postma, W.F. van Gunsteren, J. Hermans, Interaction model for water in relation to protein hydration, in: B. Pullman (Ed.), Intermolecular Forces, D. Reidel Publishing Company, Dordrecht, The Netherlands, 1981.
[44] H.J.C. Berendsen, J.P.M. Postma, W.F. van Gunsteren, A.D. Nola, J.R. Haak, Molecular dynamics with coupling to an external bath, J. Chem. Phys. 81 (1984) 3684–3690.
[45] L.B. Hess, H. Bekker, H.J.C. Berendsen, J.G. Fraaije, LINCS: a linear constraint solver for molecular simulations, J. Comput. Chem. 18 (1997) 1463–1472.
[46] W.F. van Gunsteren, S.R. Billeter, A.A. Eising, P.H. Hünenberger, P. Krüger, A.E. Mark, W.R.P. Scott, I.G. Tironi, Biomolecular Simulation: The GROMOS96 Manual and User Guide, Hochschulverlag AG an der ETH Zürich, Zürich, Switzerland, 1996.
[47] S. Leavitt, E. Freire, Direct measurement of protein binding energetics by isothermal titration calorimetry, Curr. Opin. Struct. Biol. 11 (5) (2001) 560–566.
[48] A. Cooper, Heat capacity effects in protein folding and ligand binding: a re-evaluation of the role of water in bimolecular thermodynamics, Biophys. Chem. 115 (2005) 80–97.
[49] J.L. Silva, D. Foguel, A.T. Da Poian, P.E. Prevelige Jr., The use of hydrostatic pressure as a tool to study viruses and other macromolecular assemblages, Curr. Opin. Struct. Biol. 6 (1996) 166–175.
[50] J.L. Silva, D. Foguel, C.A. Royer, Pressure provides new insights into protein folding, dynamics and structure, Trends Biochem. Sci. 26 (2001) 612–618.
[51] A.P. Valente, C.A. Miyamoto, F.C. Almeida, Implications of protein conformational diversity for binding and development of new biological active compounds, Curr. Med. Chem. 13 (2006) 3697–3703.
[52] T.L. Blundell, B.L. Sibanda, R.W. Montalva, S. Brewerton, V. Chelliah, C.L. Worth, N.J. Harmer, O. Davies, D. Burke, Structural biology and bioinformatics in drug design: opportunities and challenges for target identification and lead discovery, Phil. Trans. R. Soc. B 361 (2006) 413–423.
[53] E.C. Lacasse, S. Baird, R.G. Korneluck, A.E. Mackenzie, The inhibitors of apoptosis (IAPs) and their emerging role in cancer, Oncogene 17 (1998) 3247–3259.
[54] B. Nachmias, Y. Ashhab, D. Ben-Yehuda, The inhibitor of apoptosis protein family (IAPs): an emerging therapeutic target in cancer, Semin. Cancer Biol. 14 (2004) 231–243.
[55] A. Verhagen, P.G. Ekert, M. Pakusch, J. Silke, L.M. Connolly, G.E. Reid, R.L. Moritz, R.J. Simpson, D.L. Vaux, Identification of DIABLO, a mammalian protein that promotes apoptosis by binding to and antagonizing inhibitor of apoptosis (IAP) proteins, Cell 102 (2000) 43–53.
[56] P.C. Weber, F.R. Salemme, Applications of calorimetric methods to drug discovery and the study of protein interactions, Curr. Opin. Struct. Biol. 13 (2003) 115–121.
[57] V. Lafont, A.A. Armstrong, H. Ohtaka, Y. Kiso, M. Amzel, E. Freire, Compensating enthalpic and entropic changes hinder binding affinity optimization, Chem. Biol. Drug Des. 69 (2007) 413–422.
[58] G.M. Whitesides, V.M. Krishnamurthy, Designing ligands to bind proteins, Q. Rev. Biophys. 38 (2005) 385–395.
[59] M.S. Celej, G.G. Montich, G.D. Fidelio, Protein stability induced by ligand binding correlates with changes in protein flexibility, Protein Sci. 12 (2003) 1496–1506.
[60] H. Fukada, J.M. Sturtevant, F.A. Quiocho, Thermodynamics of the binding of L-arabinose and of D-galactose to the L-arabinose-binding protein of *Escherichia coli*, J. Biol. Chem. 258 (21) (1983) 13193–13198.
[61] A. Shrake, P.D. Ross, Ligand-induced biphasic protein denaturation, J. Biol. Chem. 265 (9) (1990) 5055–5059.
[62] A. Shrake, P.D. Ross, Origins and consequences of ligand-induced multiphasic thermal protein denaturation, Biopolymers 32 (8) (1992) 925–940.
[63] C.N. Pace, Energetics of protein hydrogen bonds, Nat. Struct. Mol. Biol. 16 (7) (2009) 681–682.
[64] F. Cordier, C. Wang, S. Grzesiek, L.K. Nicholson, Ligand-induced strain in hydrogen bounds of the c-Src SH3 domain detected by NMR, J. Mol. Biol. 304 (2000) 497–505.
[65] M.J. Stone, NMR relaxation studies of the role of conformational entropy in protein stability and ligand binding, Acc. Chem. Res. 34 (5) (2001) 379–388.
[66] C.D. Moore, H. Wu, B. Bolanos, S. Bergqvist, A. Brooun, T. Pauly, D. Nowlin, Structural and biophysical characterization of XIAP BIR3 G30E mutant: insights in protein dynamics and application for fragment-based drug design, Chem. Biol. Drug Des. 74 (2009) 212–223.
[67] J.M. Sturtevant, Heat capacity and entropy changes in processes involving proteins, Proc. Nat. Acad. Sci. U.S.A. 74 (6) (1977) 2236–2240.
[68] M.R. Eftink, A.C. Anusiem, R.L. Biltonen, Enthalpy-entropy compensation and heat capacity changes for protein-ligand interactions: general thermodynamic models and data for the binding of nucleotides to ribonuclease A, Biochemistry 22 (16) (1983) 3884–3896.
[69] C. Wang, N.H. Pawley, L.K. Nicholson, The role of backbone motions in ligand binding to the c-Src SH3 domain, J. Mol. Biol. 313 (2001) 873–887.
[70] L. Zidek, M.V. Novotny, M.J. Stone, Increased protein backbone conformational entropy upon hydrophobic ligand binding, Nat. Struct. Biol. 6 (1999) 1118–1121.
[71] A.L. Lee, S.A. Kinnear, A.J. Wand, Redistribution and loss of side chain entropy upon formation of a calmodulin–peptide complex, Nat. Struct. Biol. 7 (2000) 72–77.
[72] K.K. Frederick, M.S. Marlow, K.G. Valentine, A.J. Wand, Conformational entropy in molecular recognition by proteins, Nature 448 (2007) 325–330.
[73] A. Crespo, A. Fernandez, Induced disorder in protein-ligand complexes as a drug-design strategy, Mol. Pharm. 5 (3) (2008) 430–437.